NASA Technical Memorandum 87290

Tensile Behavior of Fe-40Al Alloys With B and Zr Additions

Darrell J. Gaydosh and Michael V. Nathal
Lewis Research Center
Cleveland, Ohio

Prepared for the
1986 TMS-AIME Annual Meeting
New Orleans, Louisiana, March 2-6, 1986

NASA

TENSILE BEHAVIOR OF Fe-40Al ALLOYS WITH B AND Zr ADDITIONS

Darrell J. Gaydosh and Michael V. Nathal
National Aeronautics and Space Administration
Lewis Research Center
Cleveland, Ohio 44135

SUMMARY

Both Fe-40Al and Fe-40Al-0.1Zr with and without B were produced by the hot extrusion of powdered metal. Tensile properties were determined from room temperature to 1100 K in air. All of the materials possessed some ductility at room temperature, and addition of B caused an increase in ductility and a change in fracture mode from intergranular to transgranular cleavage. At high temperatures, failure was caused primarily by the formation of grain boundary cavities in all of the alloys. The effect of Zr addition was unclear because of the complexity of the various microstructures. Comparison of air and vacuum testing at high temperatures revealed that an apparent oxidation assisted mechanism reduced high temperature ductility in these alloys, especially at 900 K.

INTRODUCTION

The B2 crystal structure aluminide intermetallic FeAl is considered a potential structural material for use at elevated temperatures. A number of investigators have examined the mechanical properties of single and polycrystalline FeAl in compression at various temperatures (refs. 1 to 4). Substoichiometric Fe-40Al (all compositions in this paper are in atomic percent, unless otherwise indicated) appears to be one of the few aluminides to have exhibited low temperature tensile ductility in polycrystalline form. Sainfort et al. (refs. 5 and 6) tensile tested polycrystals of Fe-40Al over a range of temperatures in air at a strain rate of 1×10^{-3} s^{-1}. The material was cast, hot worked, and heat treated to produce a grain size of about 100 μm. The elongation of this material was 8 percent at room temperature and increased almost linearly to 60 percent at 1220 K. Yield strength remained relatively constant at 245 MPa up to 920 K, and dropped to 60 MPa at 1120 K, while the ultimate tensile strength dropped from 765 MPa at 373 K to 80 MPa at 1120 K. Fracture was mainly intergranular at room temperature, but transgranular cleavage at higher temperatures.

Mendiratta et al. (ref. 7) reported the tensile properties of Fe-35, -40, and -50Al, all with grain sizes of approximately 30 μm. These materials were produced by hot extrusion of rapidly solidified powder. The strain to failure for Fe-40Al rose from 2.5 percent at room temperature to a maximum of approximately 23 percent at 773 K, after which it dropped steadily to 12 percent at 973 K. Reduction in area also reached a maximum at 773 K, above which it decreased. Yield strength dropped slowly from 625 MPa at room temperature to about 450 MPa at 873 K, after which it decreased rapidly. Fracture was transgranular cleavage at room temperature, transgranular dimples up to 773 K, and an increasing proportion of intergranular cavities up to 973 K, which was the highest test temperature.

This paper presents the results of an investigation of the tensile behavior as a function of temperature for four B2 iron aluminides with small

ternary and quaternary additions; Fe-40Al, Fe-40Al-0.4B, Fe-40Al-0.1Zr, and Fe-40Al-0.1Zr-0.4B (hereafter denoted simply as FeAl, FeAlB, FeAlZr, and FeAlZrB, respectively). The materials were produced by hot extrusion of powdered metal, and tested in tension from room temperature to 1100 K in air, and at 900 and 1100 K in vacuum. In addition to microstructural characterization of the extruded material and the determination of tensile properties, SEM fractography and optical and SEM examination of longitudinal sections of tested specimens were used to characterize the tensile behavior.

MATERIALS AND PROCEDURES

The materials used in this study were produced by the hot extrusion of powdered metal. The powders were commercially procured as -80 mesh gas atomized powder, the compositions of which are shown in table I. It should be noted from this table that the Fe-40Al powders contained significant amounts of unwanted trace elements. The two B containing alloys were prepared by adding amorphous B powder of less than 1 μm diameter to the original powders and blending them in a vee blender for 2 hr. Chemical analysis of both extrusions confirmed that B was present at 0.4 at % (0.1 wt %).

For each alloy, approximately 500 g of powder was placed in a mild steel can of 5.1 cm diameter, 0.6 cm wall thickness, and 14 cm height. The cans were sealed under vacuum and extruded at 1250 K at a reduction ratio of 16:1. The resulting 1.3 cm diameter bars were cut into approximately 5.1 cm lengths with a dash-pot controlled abrasive saw, and heat treated at 922 K for 2 hr in Ar. The extrusion cans were removed by centerless grinding and button-head tensile specimens with a gauge diameter of 3.1 mm and a gauge length of 33.0 mm were centerless ground from the resulting cylinders to a surface finish of 0.4 μm. The specimens were then electropolished at -25 °C in a 10 percent perchloric acid in methanol solution at 10 V.

Tensile specimens were strained to failure in tension at 300, 500, 700, 900, and 1100 K in air in an Instron testing machine at a constant crosshead velocity, with an initial strain rate of 1.3×10^{-4} s^{-1}. Tension tests were also run at 900 and 1100 K in a vacuum of 1.33×10^{-4} Pa at the same constant crosshead velocity in another Instron machine. Stress and strain data were calculated from the load-time charts. Yield strength was determined using the 0.2 percent offset method when yielding was continuous, and the lower yield was reported when a sharp yield drop occurred. Percent elongation as calculated from the load-time chart agreed closely with that determined by the measured change in specimen length.

Optical metallography, x-ray diffraction, and energy dispersive spectroscopy (EDS) were used to assess the structure of the extruded, heat treated material. The materials were etched with the following mixture; 33 ml-HNO_3, 33 ml-acetic acid, 33 ml-H_2O, and 1 ml-HF. Grain size was measured using the line intercept method. The fracture surfaces of the tested specimens were examined in the SEM. Longitudinal sections produced by mounting a section of the gauge length in bakelite and grinding to mid-radius were examined in the etched and unetched conditions using optical and electron microscopy.

RESULTS

Microstructure

Optical metallography of FeAl (figs. 1(a) and (b)) and FeAlB revealed a grain boundary phase and large inclusions throughout the material. Energy dispersive spectroscopy (EDS) in the SEM indicated the presence of a high level of Ta in the grain boundary phase. FeAlB appeared to have a smaller amount of the grain boundary phase, present as discrete particles rather than as a nearly continuous grain boundary film. EDS analysis also showed that the large inclusions contained principally Cr, Co, and Ta, with low levels of Ni. Comparison of the EDS results with the chemical analysis of the as-received powders (table I) indicates the source of these unwanted phases. Figure 1(a) illustrates the relative amount of the inclusions present, which is estimated at approximately 0.9 vol %. The virtual absence of large inclusions in the Zr-containing alloys is shown in figure 2(a). The difference in the amount of inclusions between the Zr-containing alloys and the Zr-free alloys is consistent with the chemical analysis presented in table I. The presence of a fine, evenly distributed second phase was also observed in the Zr-containing alloys (fig. 2(b)). EDS verified that this second phase contained a high level of Zr. SEM observation further revealed that the addition of B decreased the size of the second phase from approximately 1 μm in FeAlZr to approximately 0.5 μm in FeAlZrB.

Optical micrographs taken under differential interference contrast (DIC) lighting conditions are shown in figures 3 and 4. In the alloys without Zr, grain boundaries were not associated with prior particle boundaries, which were marked by oxides left from the surface of the original powder particles (fig. 3). Therefore grain growth was not impeded by these boundaries. Grains were equiaxed with an average diameter of approximately 14 μm. While grain sizes ranged from 12 to 16 μm for FeAl, the grain sizes of FeAlB exhibited a greater variation in ranging from 8 to 22 μm, while still producing the same mean value of 14 μm. In contrast to the Zr-free alloys, grain growth in the two Zr-containing alloys appeared to be impeded by the prior particle boundaries, and in many cases grain boundaries and prior particle boundaries coincided. The transverse and longitudinal micrographs (fig. 4) show that wherever prior particles were large, grains grew large, and that wherever they were small, grains were likewise small. Grains therefore ranged in size from 2.5 to 25 μm. The average size of grains in areas without prior particle oxide boundaries was 13 μm, while the average size of grains in areas with many oxide boundaries was approximately 7 μm. The overall average grain size for both alloys was 9 μm, as B additions had no noticeable effect on grain size.

Finally, x-ray diffraction indicated that only FeAlZr showed any strong preferred orientation. In this alloy, the 110 axis was strongly oriented parallel to the extrusion direction.

Tensile Properties-Air

Typical stress-strain curves as a function of temperature for FeAlZr are shown in figure 5 as an example of the observed stress-strain behavior of all four alloys. Typically, a sharp yield point with a Luder's strain was observed at 300 and 500 K, followed by work hardening to failure. At 700 K a more diffuse yield drop occurred, which was followed by work hardening, and finally

necking at failure. At 900 and 1100 K smooth yielding was observed, followed by a steadily decreasing stress to failure.

The mechanical properties measured from the tensile tests are shown in figures 6 to 9. The yield strength (YS) of all of the alloys remained relatively constant at 550 to 700 MPa up to 700 K and then dropped almost linearly to 70 MPa at 1100 K. The ultimate tensile strength (UTS) reached a peak at 850 to 1200 MPa and then dropped almost linearly to 70 MPa at 1100 K. The two B containing alloys had higher yield and ultimate tensile strengths compared to the corresponding B-free alloys.

The percent elongation at room temperature ranged from 1 to 5 percent for the four alloys. The elongation then increased nearly linearly up to 12 to 20 percent at 700 K, followed by a drop in elongation at 900 K to 5 to 15 percent. Increasing the test temperature to 1100 K caused the percent elongation to again increase. Although the FeAlZrB alloy appeared to be an exception to this general behavior (fig. 8), further testing is necessary to be certain. At 300 K, the B containing alloys had larger elongation values than their sister alloys, but from 500 to 1100 K the alloys without B were superior. The reduction in area (RA) at 300 K ranged from 2 to 8 percent, and increased up to 35 to 85 percent at 700 K. Increasing the temperature from 700 to 1100 K decreased the RA to 10 to 35 percent. Again, a crossover was evident as the B containing alloys possessed a greater RA at room temperature, but lower RA values above 500 K.

Failure Mechanisms

Macro photographs of the tested specimens of FeAl and FeAlZr are in figure 10. Note how necking becomes prominent at the intermediate temperatures, before disappearing at the highest temperatures. Because oxidation partially obscured the fracture surfaces at 900 and 1100 K, SEM fractographs of air tested specimens are only presented for test temperatures up to 700 K.

Failure at 300 and 500 K. - The failure in FeAl was intergranular at 300 and 500 K, as shown in figure 11. The irregularities seen on the grain facets (indicated by the arrow in fig. 11(a)) are due to the Ta grain boundary phase. Only minor cracking of the large inclusions occurred at these temperatures. FeAlB failed by transgranular cleavage at these two temperatures, with the B addition strengthening the grain boundaries and eliminating intergranular failure (fig. 12). Some minor cracking of the large inclusions again occurred.

FeAlZr, like FeAl, exhibited intergranular failure at 300 and 500 K (fig. 13). Note the areas of large and small grains and the prior particle boundaries marked by the arrows in the fractograph in figure 13(a). Fractographs taken at higher magnifications revealed small protrusions and corresponding holes on the grain boundary facets which were caused by the second phase particles that resided on the grain boundaries. Because the size and number of the inclusions in FeAlZr was so small, virtually no cracking of inclusions was observed. However, cracking of the Zr rich second phase particles and the matrix-particle interfaces occurred in this temperature range, to a greater degree at 500 K (fig. 13(b)). Again, the addition of B in FeAlZrB strengthened the grain boundaries and caused a change in fracture mode from intergranular to transgranular cleavage, as shown in figure 14. Cracking of

the second phase particles and matrix-particle interfaces also occurred at 500 K.

Failure at 700 K. - Figure 15(a) shows that at 700 K the cracks in the inclusions and at the matrix-inclusion interfaces in FeAl grew into large voids because of the large deformation in the surrounding matrix. The fracture was a combination of the separation of grain boundaries or prior particle boundaries that were parallel to the longitudinal direction, and a transgranular cleavage type failure in the transverse direction, with some evidence of dimpled ductile rupture or cavitation (fig. 15(b)). The longitudinal section in figure 15(c) shows that some individual grains separated and necked (as indicated by the arrow). Some separation of transverse grain boundaries also occurred at this temperature. FeAlB behaved similarly to FeAl at 700 K, and the longitudinal sections and fracture surfaces were nearly identical. The only difference between the two alloys was the B addition in FeAlB appeared to eliminate any transverse grain boundary separation.

The absence of inclusions and associated cracking and void formation in FeAlZr is evident in the unetched longitudinal section in figure 16(a). The fracture surface of FeAlZr at 700 K consisted of two distinct areas, the first of which was a transgranular fracture consisting of flat cleavage facets. The second area represented the final failure and consisted primarily of transgranular cleavage, along with some longitudinal grain boundary and prior particle boundary separation (fig. 16(b)). Cracking of the second phase particles and the matrix-particle interfaces was also observed at this temperature, while separation of transverse grain boundaries was not observed. The B addition in FeAlZrB appeared to have no effect at this temperature, as the longitudinal sections and fracture surfaces were nearly identical to those of FeAlZr. The cracking of the second phase particles and their interfaces in FeAlZrB is shown in figure 16(c).

Failure at 900 and 1100 K. - In FeAl tested at 900 K, cavitation occurred throughout the matrix near the fracture surface, and the cavitation was more extensive and extended further away from the fracture surface at 1100 K. The extent of the cavitation at 1100 K can be seen in the unetched longitudinal section in figure 17(a). Figures 17(b) and (c) show that the cavitation occurred on the grain boundaries at both temperatures, and that the failure occurred primarily by the growth and linkage of these grain boundary cavities. FeAlB failed in an identical manner at 900 and 1100 K.

Cavitation occurred in a similar way in FeAlZr (fig. 18) and FeAlZrB (fig. 19) at 900 and 1100 K. (It should be noted that the apparent difference in the amount of cavitation between figs. 17(a) and 18(a) is probably due to different polishing techniques and is not a real effect.) Very little cracking of the second phase particles or their matrix interfaces was observed in the matrix at these two temperatures. Although some voids appeared at particle-matrix interfaces, cavitation still took place primarily on grain boundaries. Observation of the longitudinal sections of these two alloys revealed bands where little or no cavitation occurred, especially at 900 K (indicated by the arrow in fig. 19(a)). It appeared that these bands were areas where there were no prior particle boundaries, i.e., areas with larger grains.

Some preliminary results of elevated temperature testing in vacuum are presented below. These tests were done at 900 K for FeAl and FeAlB, and at 900 and 1100 K for FeAlZr and FeAlZrB. Further vacuum testing is in progress.

The percent elongation and reduction in area results for the vacuum tensile tests are presented in figures 20 and 21, along with the respective results from the air testing. Because the YS and UTS values never differed from the air tested values by more than 20 and 40 MPa, respectively, they are considered to be the same and are not shown here.

For FeAl and FeAlB, testing in vacuum increased the percent elongation at 900 K by 4 and 9 percent, respectively. For FeAlZr, testing in vacuum increased the percent elongation at both 900 and 1100 K, eliminating the ductility minimum observed in air. For FeAlZrB, the percent elongation was higher at 900 K and nearly the same at 1100 K. For all of the alloys, testing in vacuum resulted in an increased RA at 900 K, while no difference between vacuum and air testing at 1100 K was observed for FeAlZr and FeAlZrB (FeAl and FeAlB have not been tested at 1100 K).

Examination of the fracture surfaces of FeAl and FeAlB tested in vacuum at 900 K revealed a mixture of transgranular cleavage and grain boundary cavitation (fig. 22). For FeAlZr at 900 K, the fracture surface consisted entirely of cavitation (fig. 23(a)). Although the fracture features were partially obscured at 1100 K, perhaps due to the evaporation of aluminum, the failure appeared to be intergranular (fig. 23(b)). For FeAlZrB (fig. 24), the presence of cavitation was again observed at 900 K, although it was much less pronounced than in FeAlZr at 900 K. The fracture at 1100 K appeared identical to that for FeAlZr at the same temperature.

DISCUSSION

General Tensile Deformation Behavior

The failure of the alloys at 300 and 500 K was by the separation of grain boundaries in the B free alloys and the propagation of transgranular cleavage cracks in the B containing alloys. Cracking of the harder inclusions and second phases and the matrix-particle interfaces was observed at these temperatures. The increase in UTS from 300 K to a peak at 500 K in all four alloys was due to an increased amount of elongation, which allowed more strain hardening before failure. (It should be noted that, while the work of Mendiratta et al. (ref. 7) and Sainfort et al. (ref. 5) are discussed here, these researchers have only tested binary FeAl, and have not considered other alloying additions.) Mendiratta et al. (ref. 7) observed higher elongation values and a similar yield strength in Fe-40Al with a grain size of 33 μm that was also extruded from powdered metal. Sainfort et al. (ref. 5) reported much greater elongation in cast and extruded Fe-40Al with a 100 μm grain size, while YS was about 50 percent lower. The large grain size may be responsible for the increased elongation and reduced YS when compared to the powder metallurgy alloys.

The failure at 700 K occurred after large amounts of strain and pronounced necking. Final failure occurred by the separation of longitudinal boundaries, followed by some necking of individual grains and by transgranular cleavage. In addition, some evidence of dimpled ductile rupture was observed in the Zr free alloys. Cracking of the inclusions and their matrix interfaces again occurred in these alloys, while cracking of the second phase particles and their matrix interfaces occurred in the Zr containing alloys. It is interesting to note that Mendiratta et al. (ref. 7) observed transgranular dimples at

this temperature, while Sainfort et al. (ref. 5) observed transgranular cleavage. YS remained approximately the same as that at 500 K, while the UTS decreased because strain hardening was greatly reduced by thermally activated recovery processes. The large increase in RA from 500 to 700 K, accompanied by the pronounced necking at 700 K, was consistent with the decrease in strain hardening.

Increasing the temperature to 900 and 1100 K resulted in two changes in the failure mechanisms. First, grain boundary cavitation became the primary cause of failure, and it became more extensive as the temperature was increased from 900 to 1100 K. Mendiratta et al. (ref. 7) also reported the presence of intergranular cavitation from 773 to 973 K. Because the failure in the vacuum tested, Zr free alloys at 900 K was a mixture of transgranular cleavage and grain boundary cavitation, it appears that 900 K was a transition temperature between transgranular cleavage at intermediate temperatures (700 K) and intergranular cavitation at high temperature (1100 K). Although the vacuum tested, Zr containing alloys failed completely by cavitation at 900 K, a similar transition may have occurred at a lower temperature (~800 K). Cracking of the second phase particles in the matrix of the Zr containing alloys was rarely seen at these temperatures. The YS and UTS of all of the alloys began to converge at 900 K, and did converge at 1100 K, as strain hardening disappeared. The presence of intergranular cavitation reduced the tendency for necking and kept the RA from increasing above 900 K. Finally, it is interesting to note that YS and UTS of these alloys and those of Sainfort et al. (ref. 5) had the same value of approximately 70 MPa at 1100 K. However, Sainfort et al. (ref. 5) did not observe cavitation or a ductility minimum, evidently due to the larger grain size of their material.

The second change that occurred along with the appearance of cavitation was an oxidation effect that was most noticeable at 900 K. Testing in vacuum (figs. 21 and 22) at 900 and 1100 K generally resulted in higher elongations than for testing in air. Reductions in area were higher at 900 K in all four alloys, and were identical to the air tested values at 1100 K for the two alloys tested. The air environment decreases elongation and reduction in area at 900 K, apparently as a consequence of an oxidation assisted failure mechanism. However, as the temperature is increased further to 1100 K, grain boundary cavitation appears to become predominant over any surface effects. This results in the ductility values from air tests becoming equivalent to those of vacuum tests at 1100 K. Liu et al. (ref. 8) reported a much larger ductility increase in the $L1_2$ aluminide Ni-24Al-0.2B at 873 K in tension testing when the test environment was changed from air to vacuum. This was accompanied by a change in fracture mode from intergranular failure in air to transgranular cleavage failure in vacuum. The effect of the air environment was stated to be a dynamic interaction of air with the deforming material at high temperature, and not just an effect of oxidation per se. Although there was no change in fracture mode in the FeAl's tested in vacuum similar to that observed by Liu et al. (ref. 8), similar reasoning may still apply in the present case. Further testing is required to understand this effect of air on the tensile behavior at elevated temperature.

If the oxidation effect is removed, then the elongation of the alloys may increase steadily with temperature up to at least 1100 K, as shown for FeAlZr in figure 20(b). Even though the elongation values continue to increase, the leveling off of reduction in area at 900 K, and the decrease in reduction in area at 1100 K are consistent with the dominance of cavitation at these two

temperatures. Failure by cavitation occurred without significant necking, so that the RA values were not as high.

B Effect

The addition of B to FeAl and FeAlZr caused a change in fracture mode at 300 and 500 K from intergranular separation to transgranular cleavage. Accompanying this change in fracture mode was an increase in YS, UTS, elongation, and RA. The presence of B probably causes an increase in both strength and ductility at these temperatures because it increases the fracture strength of the grain boundaries, thus enabling more deformation and cleavage failure within the grains. At 700 K, B eliminated transverse grain boundary separation in FeAl. Both the YS and UTS of the B containing alloys remained higher at this temperature, while the elongation and RA values crossed over and fell below those for the B free alloys. At 900 and 1100 K, the YS and UTS continued to be superior for the B containing alloys, while the ductility decreased still further below that of the B free alloys. This decrease in ductility is apparently the result of easier cavitation in the B containing alloys. One possible mechanism could involve B pinning of the grain boundaries, thus preventing grain boundary sliding and causing an earlier onset of cavitation. An additional mechanism may be solid solution strengthening of the matrix by B. However, it is recognized that further work is necessary to clarify the effect of B, including the influence of an air environment on the fracture process.

Zr Effect

The addition of Zr to FeAl and FeAlB increased the YS and UTS values at 300 and 500 K, and decreased the two strengths from 700 to 1100 K. The addition of Zr also increased the ductility of both alloys over the entire temperature range, with the magnitude of the increase becoming greater with increasing temperature. At low temperature FeAlZr had greater strength and ductility than FeAl, even though both alloys failed intergranularly.

It is difficult to clarify the effects of Zr because of the complexity of the various microstructures. The influences of the significantly lower impurity level and consequent lower inclusion content of the Zr containing alloys cannot be separated from the effects of the Zr-rich second phase particles. Furthermore, the grain size and texture of the various alloys differed to some extent. However, Zr segregation to grain boundaries in a manner analagous to Zr and B segregation in other materials (ref. 9) is probably important. A contribution from solid solution hardening of the matrix by Zr and B cannot be ruled out, either. Finally, although there was no apparent synergistic effect of combined addition of Zr and B, Mantravadi et al. (ref. 10) did observe a synergistic effect of Zr and B in these same alloys tested in compressive creep.

The presence of the cavity free bands in the Zr containing alloys tested at 900 and 1100 K (fig. 19(a)) could be due to a grain size effect, with small grained areas being more susceptible to the formation of cavities. An alternative explanation is that more oxides are present in small grained areas, and that these oxides enhance cavitation.

SUMMARY OF RESULTS

1. FeAl and FeAlB contained impurities which resulted in a Ta rich grain boundary phase and 0.9 vol. % of large inclusions containing Cr, Co, and Ta. Addition of B appeared to change the shape of the grain boundary phase from a nearly continuous grain boundary film to discrete particles. FeAlZr and FeAlZrB contained very few inclusions, and a Zr rich second phase present as fine particles. Addition of B reduced the size of the second phase from approximately 1.0 μm to approximately 0.5 μm.

2. At low temperatures, the addition of B changed the fracture mode from intergranular separation to transgranular cleavage, and increased both strength and ductility. This is consistent with B segregating to and strengthening the grain boundaries. The addition of B strengthened both FeAl and FeAlZr at all temperatures, while decreasing the ductility above 500 K. The decreased ductility above 700 K is apparently due to earlier onset of cavitation.

3. The addition of Zr to FeAl and FeAlB increased the strength at low temperature, decreased the strength at high temperature, and increased the ductility throughout the temperature range. The reasons for this behavior were unclear due to the presence of impurities, variation in grain size and texture, and variation in size of the second phase.

4. For specimens tested in air, a minimum in elongation occurred at 900 K. Testing in vacuum eliminated the decrease in elongation and further increased the reduction in area. Oxidation assisted failure appeared to be dominant at 900 K, while cavitation became more important at 1100 K.

REFERENCES

1. T. Yamagata and H. Yoshida: Mater. Sci. Eng., 1973, vol. 12, pp. 95-100.

2. R.C. Crawford and I.L.F. Ray: Philos. Mag., 1977, vol. 35, pp. 549-565.

3. Y. Umakoshi and M. Yamaguchi: Philos. Mag. A, 1980, vol. 41, pp. 573-588.

4. J.D. Whittenberger: Mater. Sci. Eng., 1983, vol. 57, pp. 77-85.

5. G. Sainfort, P. Mouturat, Mme. P. Pepin, J. Petit, G. Cabane, and M. Salesse: Mem. Sci. Rev. Metall., 1963, vol. 60, pp. 125-134.

6. G Sainfort, J. Gregoire, P. Mouturat, and M. Romeggio: in Fragilite et Effects de L'irradiation, M. Salesse and M. Chaudron, eds., pp. 187-198, Presses Universitaires de France, Paris, France, 1971.

7. M.G. Meniratta, S.K. Ehlers, and D.K. Chatterjee: in Rapid Solidification Processing-Materials and Technologies III, Robert Mehrabian, ed., National Bureau of Standards, Gaithersburg, MD, 1982.

8. C.T. Liu, C.L. White, and E.H. Lee: Scr. Metall., 1985, vol. 19, pp. 1247-1250.

9. R.T. Holt and W. Wallace: Int. Met. Rev., 1976, vol. 21, pp. 1-24.

10. N. Mantravadi, K. Vedula, and D. Gaydosh: to be published in proceedings of the "Alternate Alloying for Environmental Resistance" symposium, 115th TMS-AIME meeting, March 2-6, 1986, New Orleans, Louisiana.

TABLE I. - POWDER COMPOSITION, ATOMIC PERCENT

	Fe	Al	Zr	Ta	Cr	Co	Mn
Fe-40Al	59.7	40.0	----	0.07	0.09	0.06	0.08
Fe-40Al-0.1Zr	59.5	40.3	0.12	----	.01	.05	----
	H[a]	N[a]	O[a]				
Fe-40Al	10	27	570				
Fe-40Al-0.1Zr	10	17	450				

[a]ppm by weight.

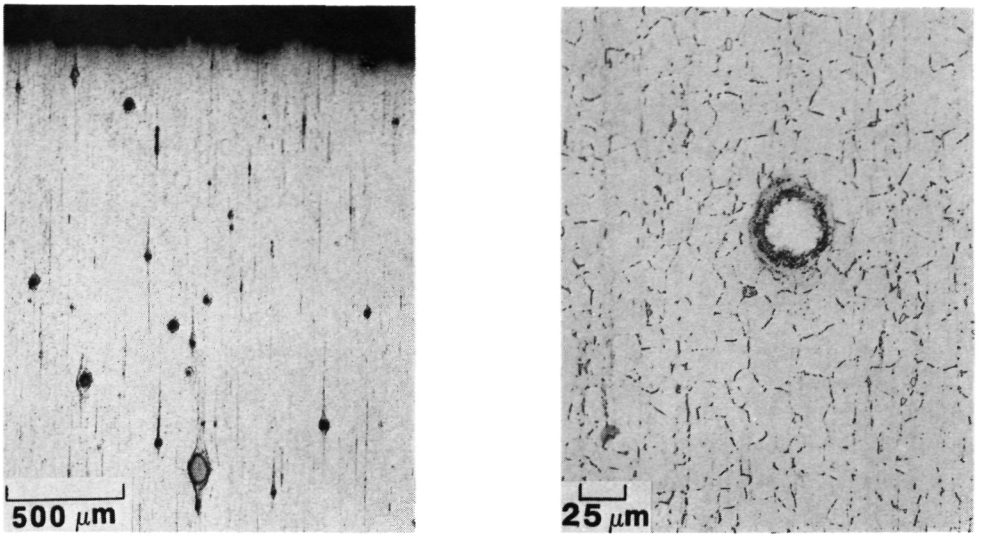

(a) (b)

Figure 1. - Optical photomicrographs of FeAl in the etched condition, showing the presence of large inclusions and a Ta-rich grain boundary phase. Treated at 922 K for 2 hours.

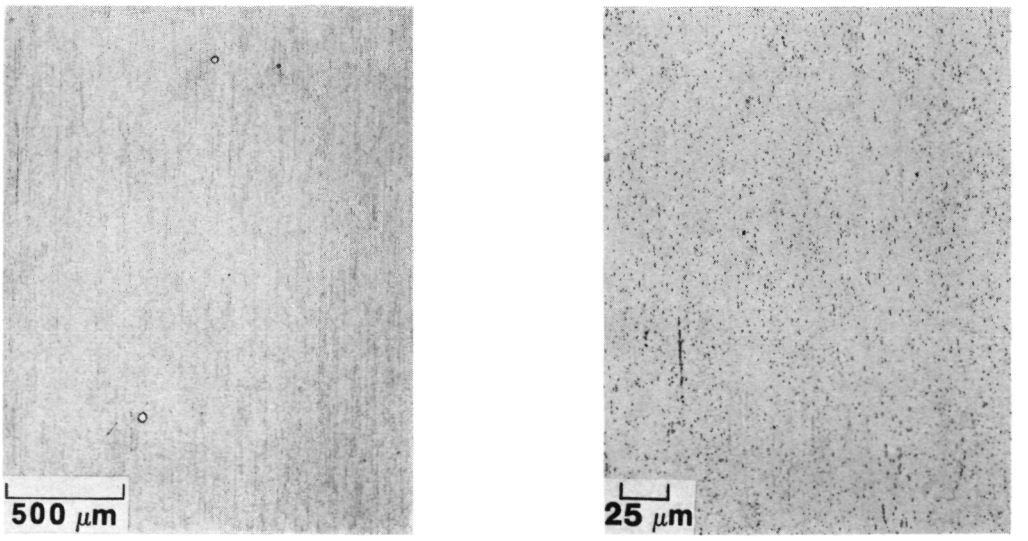

(a) (b)

Figure 2. - Optical photomicrographs of FeAlZr in the etched condition, showing the absence of inclusions and the presence of a fine second phase. Treated at 922 K for 2 hours.

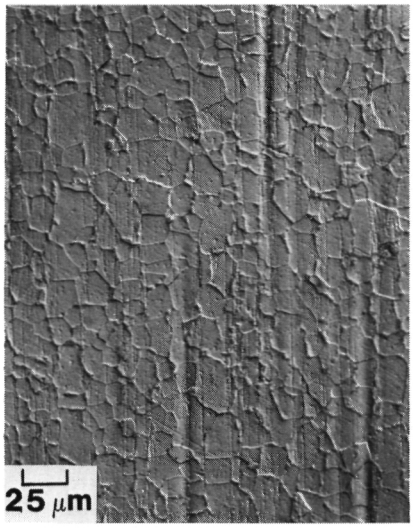

Figure 3. - Optical photomicrograph of FeAl in the etched condition, showing equiaxed grains. Treated at 922 K for 2 hours. Photographed under DIC lighting.

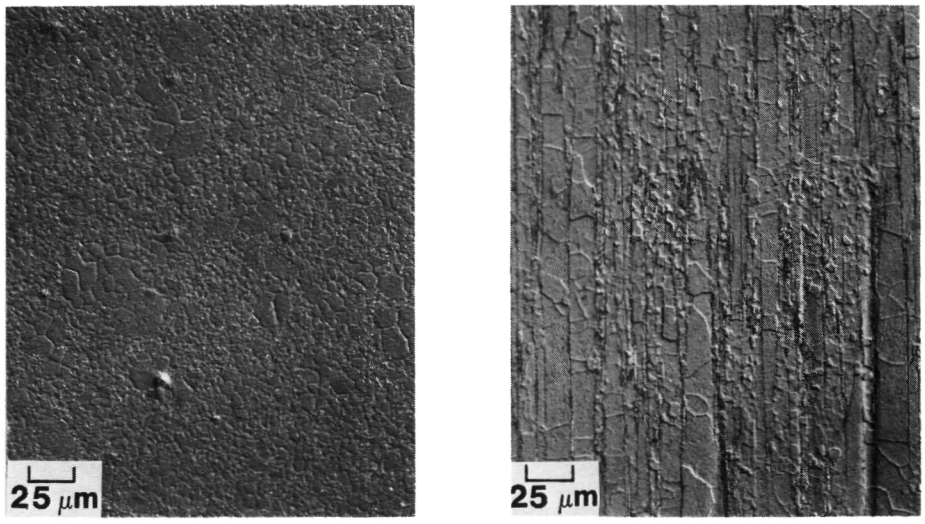

(a) (b)

Figure 4. - Optical photomicrograph of FeAlZrB in the etched condition, showing that grain boundaries and prior particle boundaries coincide. Treated at 922 K for 2 hours. Photographed under DIC lighting.

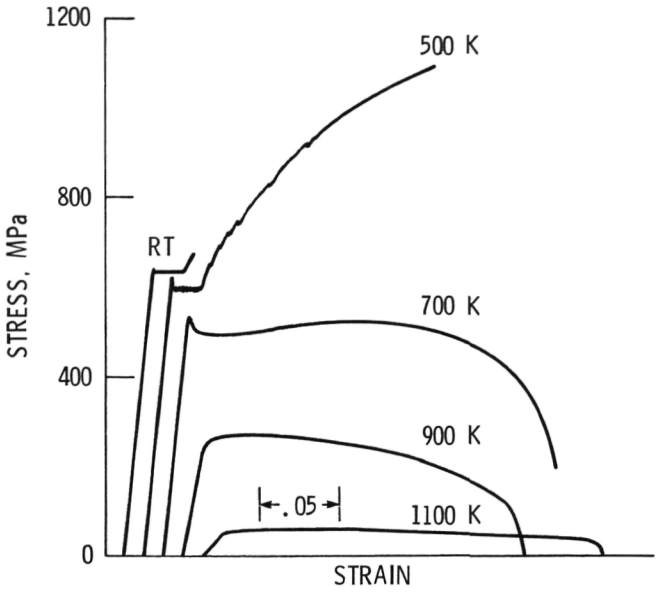

Figure 5. - Engineering stress-strain curves for FeAlZr as a function of temperature.

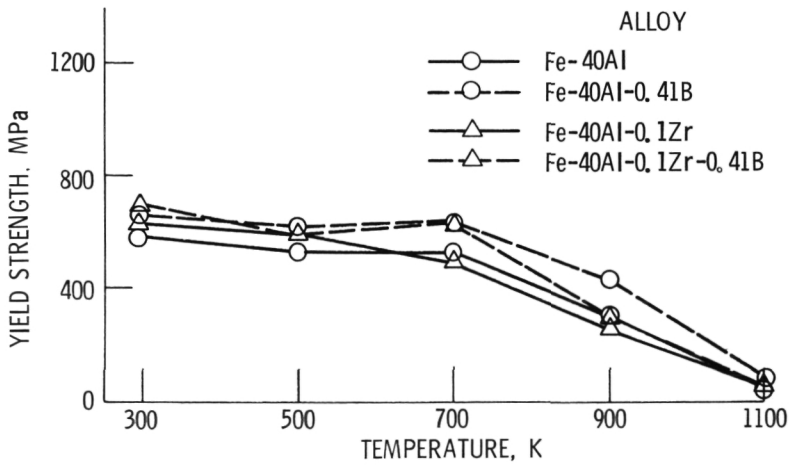

Figure 6. - Yield strength as a function of temperature for FeAl, FeAlB, FeAlZr, and FeAlZrB tested in tension at an initial strain rate of $1.3 \times 10^{-4}\ s^{-1}$ in air.

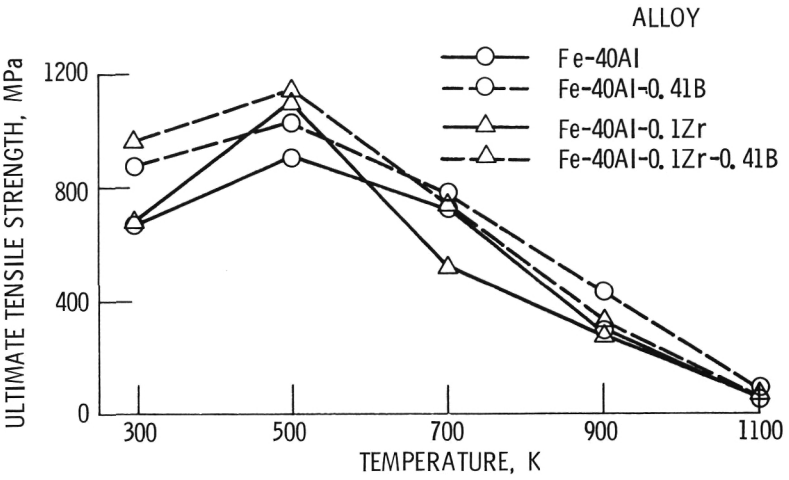

Figure 7. - Ultimate tensile strength as a function of temperature for FeAl, FeAlB, FeAlZr, and FeAlZrB tested in tension at an initial strain rate of $1.3 \times 10^{-4}\ s^{-1}$ in air.

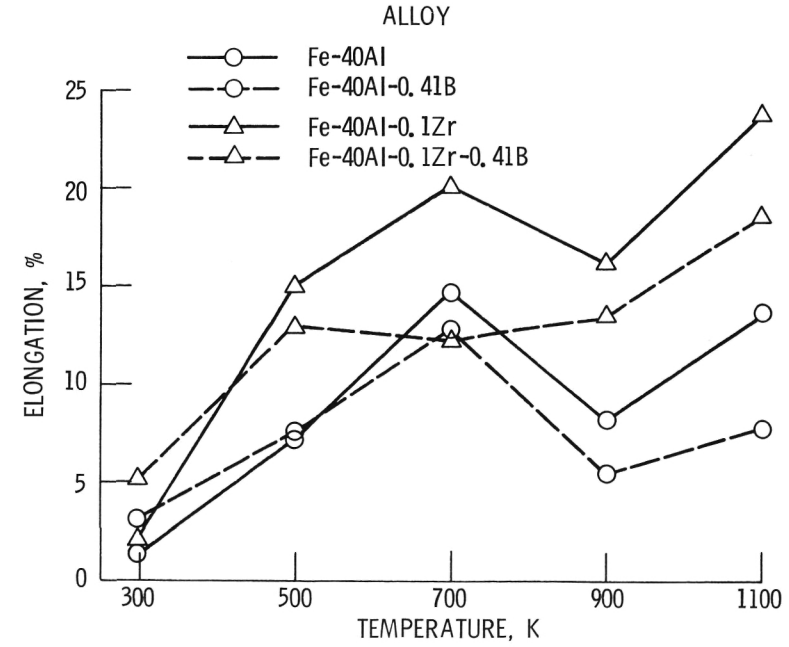

Figure 8. - Elongation as a function of temperature measured from specimens of FeAl, FeAlB, FeAlZr, and FeAlZrB tested in tension at an initial strain rate of $1.3 \times 10^{-4}\ s^{-1}$ in air.

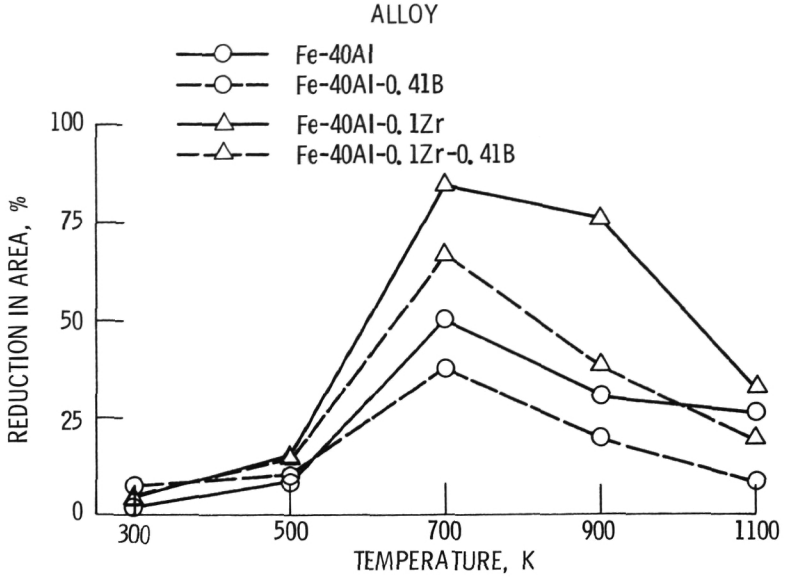

Figure 9. - Reduction in area as a function of temperature measured from specimens of FeAl, FeAlB, FeAlZr, and FeAlZrB tested in tension at an initial strain rate of $1.3 \times 10^{-4}\ s^{-1}$ in air.

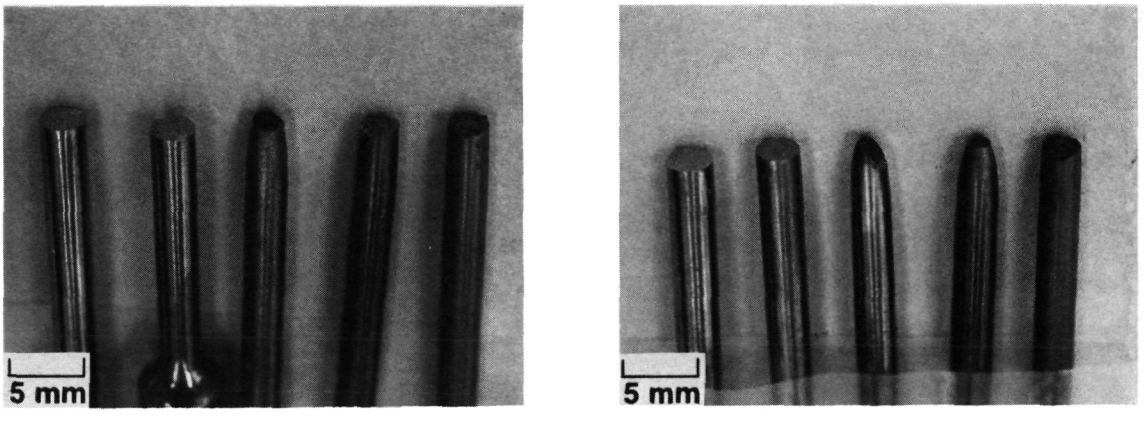

(a) (b)

Figure 10. - Photographs of the tested specimens of (a) FeAl and (b) FeAlZr. Tests were run in air at 300, 500, 700, 900, and 1100 K, from left to right. Ductility reached a maximum at 700 K.

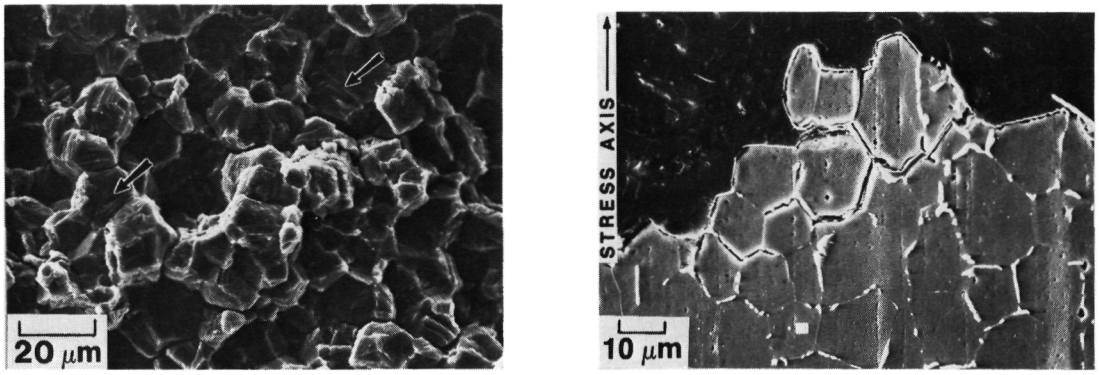

(a) (b)

Figure 11. - (a) SEM fractograph and (b) longitudinal section SEM micrograph of FeAl tested in air at 300 K, showing intergranular failure. Arrows indicate irregularities on grain facets caused by the Ta grain boundary phase.

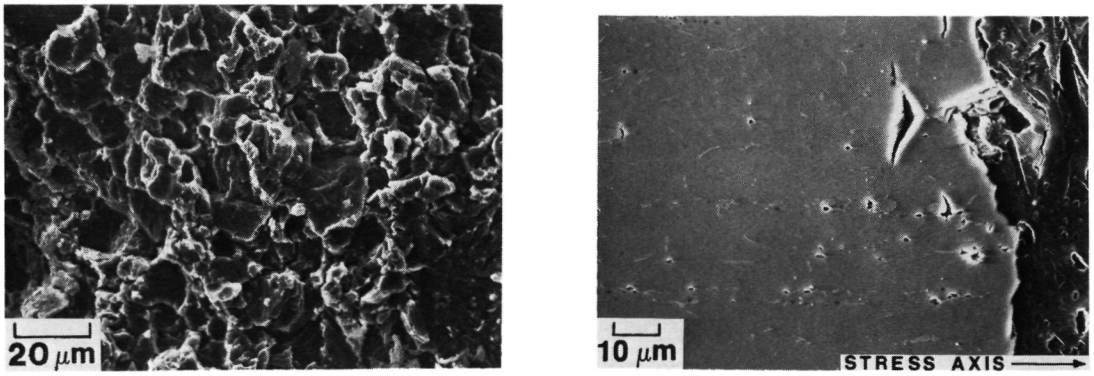

(a) (b)

Figure 12. - (a) SEM fractograph and (b) longitudinal section SEM micrograph of FeAlB tested in air at 300 K, showing transgranular cleavage failure.

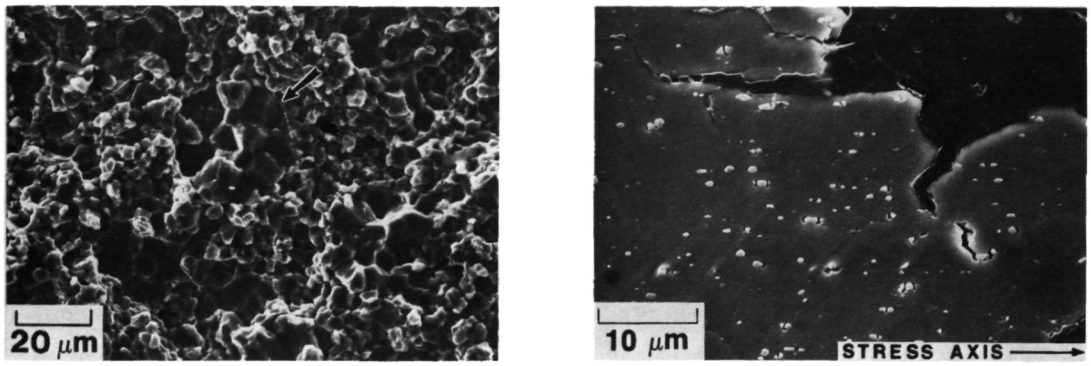

(a) (b)

Figure 13. - (a) SEM fractograph of FeAlZr tested in air at 300 K, and (b) longitudinal section SEM micrograph of FeAlZr tested in air at 500 K, showing intergranular failure and cracking of second phase particles. Arrow indicates prior particle boundary.

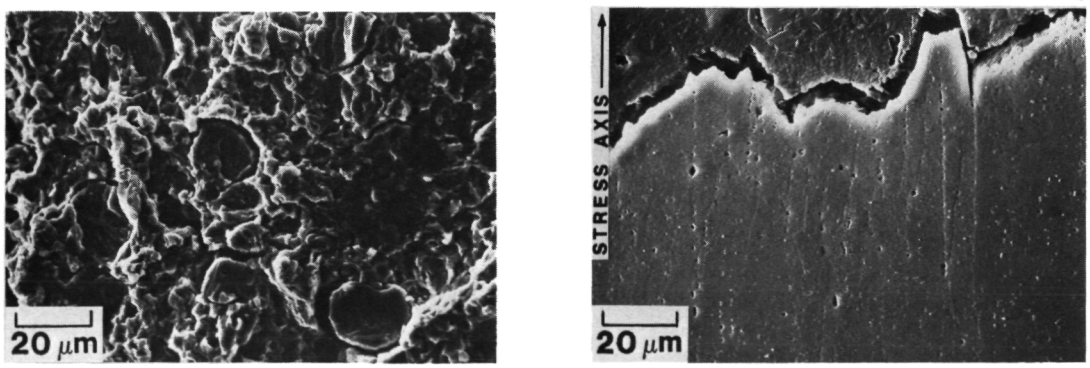

(a) (b)

Figure 14. - (a) SEM fractograph of FeAlZrB tested in air at 300 K, and (b) longitudinal section SEM micrograph of FeAlZrB tested in air at 500 K, showing transgranular cleavage failure.

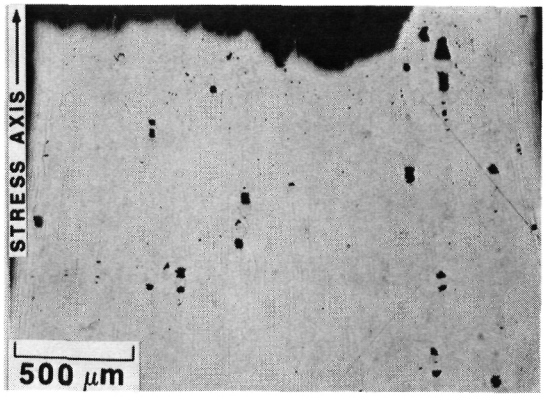

(a)

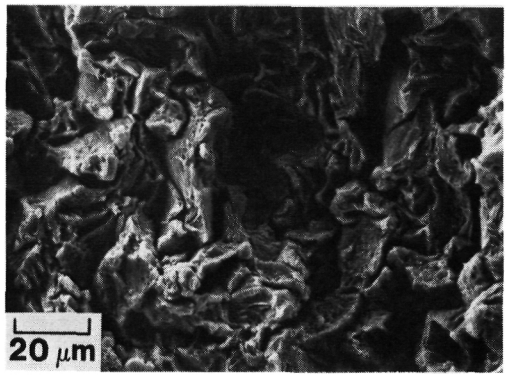

(b)

Figure 15. - (a) Optical micrograph of the unetched longitudinal section, (b) SEM fractograph, and (c) SEM micrograph of the etched longitudinal section of FeAl tested in air at 700 K. The arrow indicates the separation and necking of an individual grain.

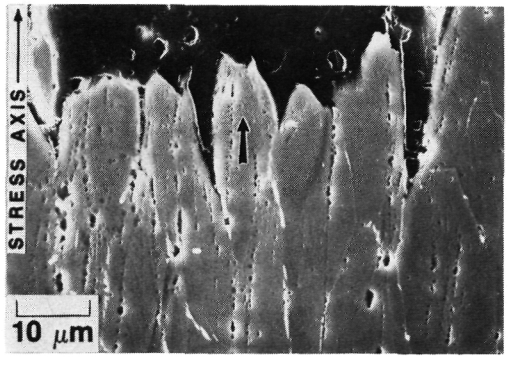

(c)

Figure 15. - Concluded.

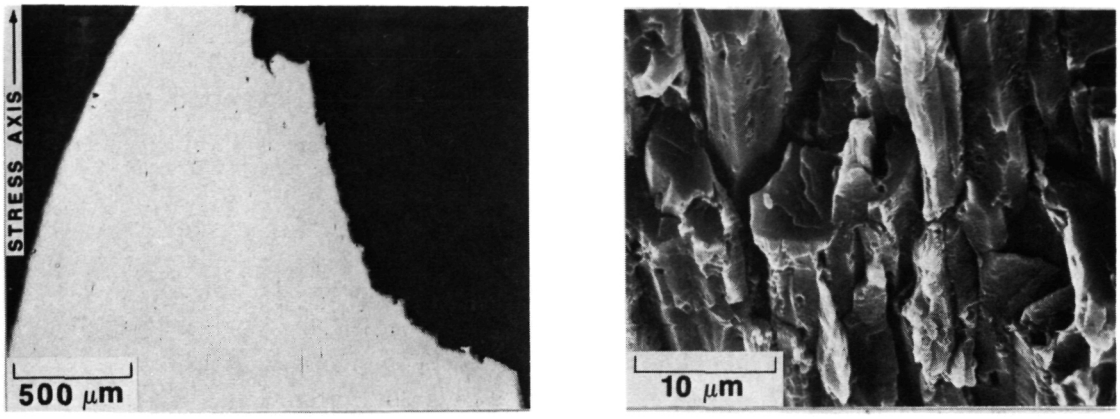

(a) (b)

Figure 16. - (a) Optical micrograph of the unetched longitudinal section, (b) SEM fractograph, and (c) SEM micrograph of the etched longitudinal section of FeAlZr tested in air at 700 K, showing transgranular cleavage and the separation of longitudinal grain boundaries.

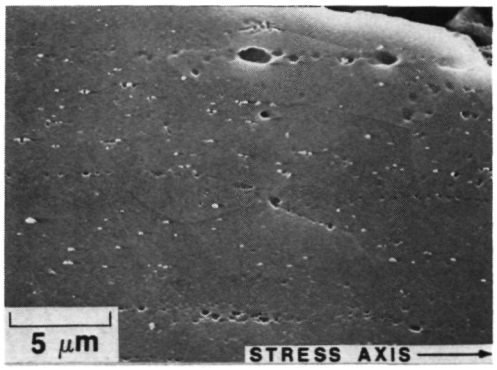

(c)

Figure 16. - Concluded.

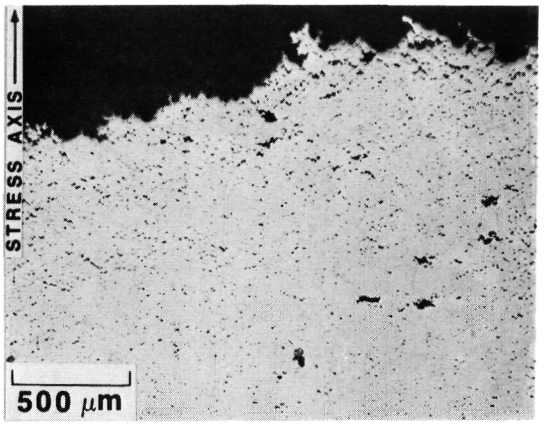

(a)

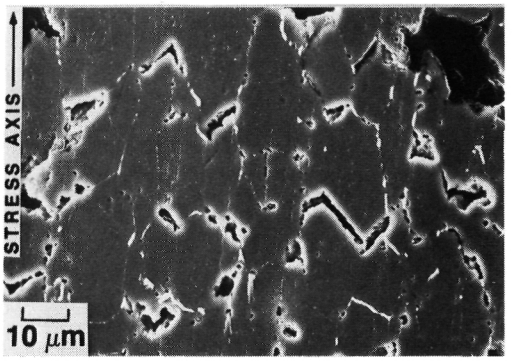

(b)

Figure 17. - (a) Optical micrograph of the unetched longitudinal section of FeAl tested in air at 1100 K, (b) SEM micrograph of the etched longitudinal section of FeAl tested in air at 900 K, and (c) SEM micrograph of the etched longitudinal section of FeAl tested in air at 1100 K, showing the formation of grain boundary cavities.

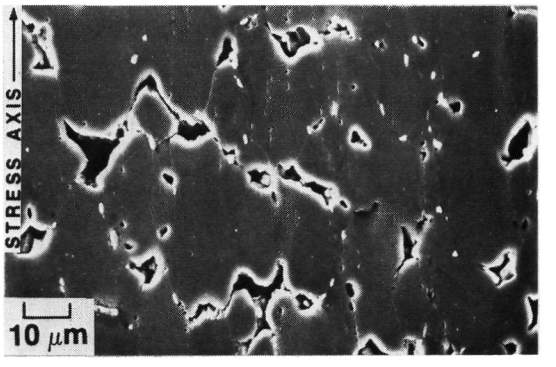

(c)

Figure 17. - Concluded.

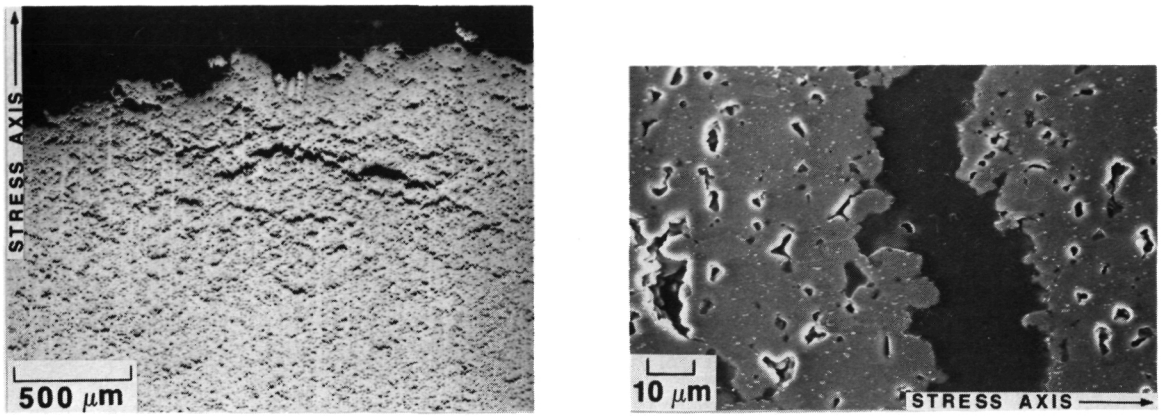

(a) (b)

Figure 18. - (a) Optical micrograph of the unetched longitudinal section, and (b) SEM micrograph of the etched longitudinal section of FeAlZr tested in air at 1100 K, again showing the formation of grain boundary cavities.

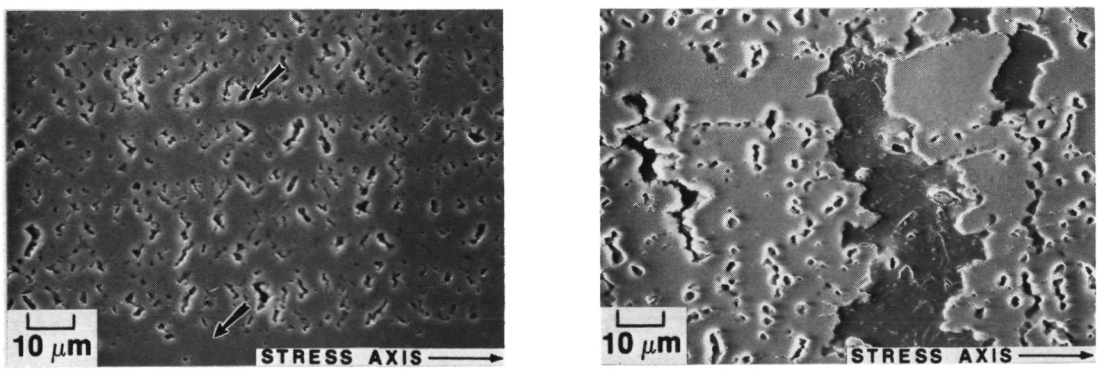

(a) (b)

Figure 19. - SEM micrographs of the unetched longitudinal sections of FeAlZrB tested in air at (a) 900, and (b) 1100 K. Arrows indicate bands where no cavitation occurred.

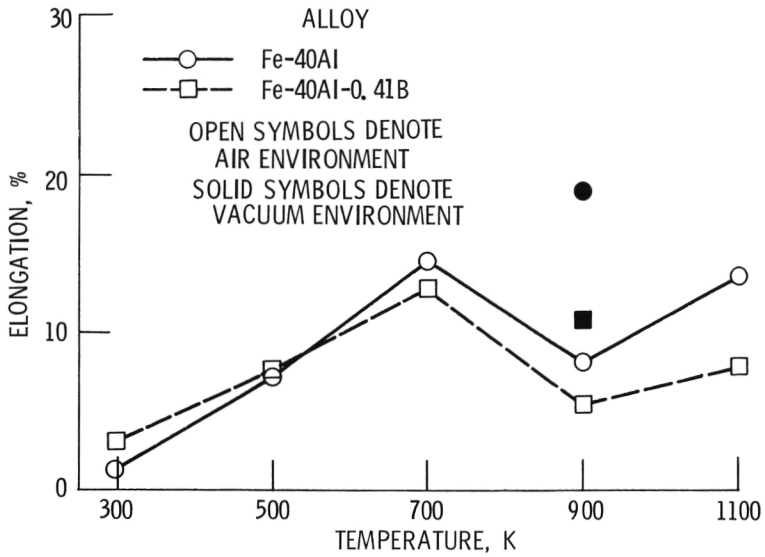

(a) FeAl and FeAlB.

Figure 20. - Elongation as a function of temperature measured from specimens tested in tension at an initial strain rate of $1.3 \times 10^{-4}\ s^{-1}$ in air and vacuum.

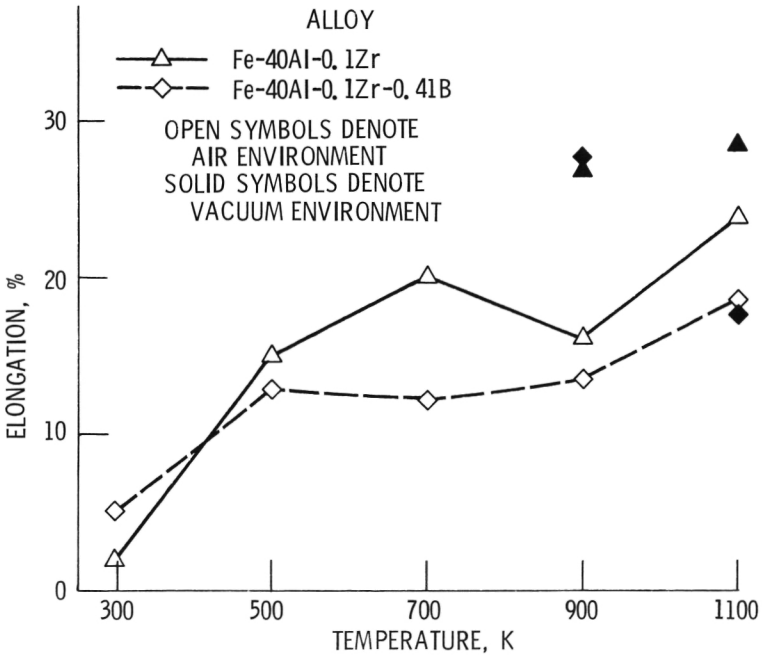

(b) FeAlZr and FeAlZrB.

Figure 20. - Concluded.

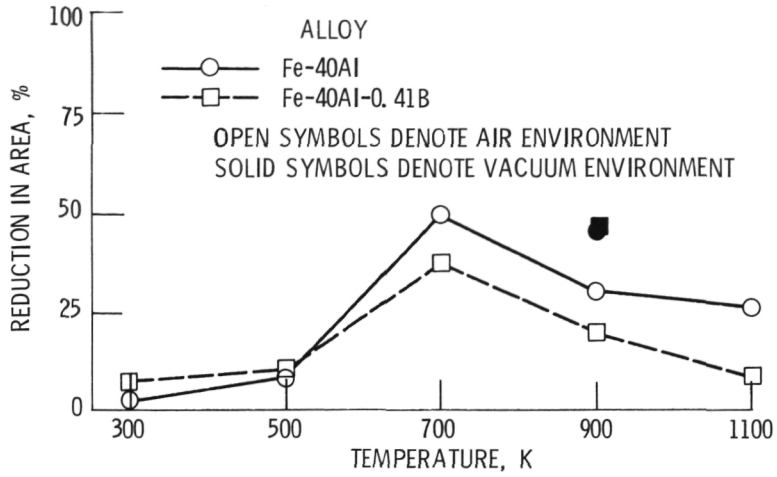

(a) FeAl and FeAlB.

Figure 21. - Reduction in area as a function of temperature measured from specimens tested in tension at an initial strain rate of $1.3 \times 10^{-4}\ s^{-1}$ in air and vacuum.

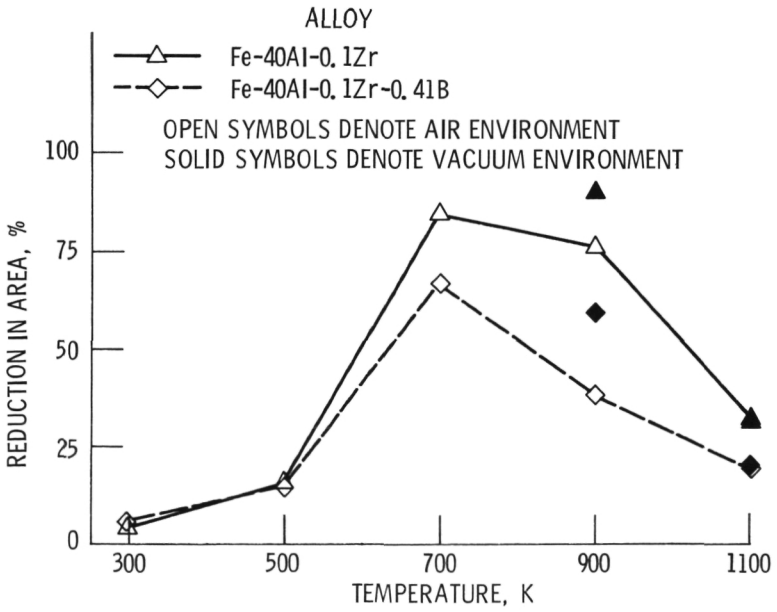

(b) FeAlZr and FeAlZrB.

Figure 21. - Concluded.

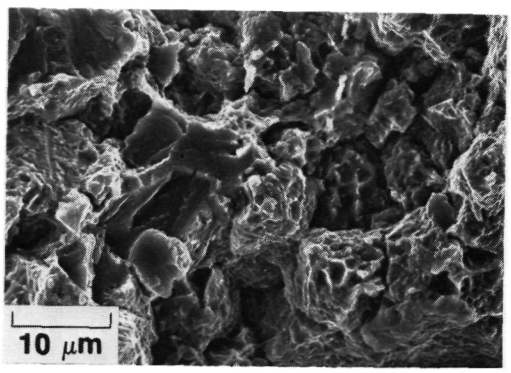

Figure 22. - SEM fractograph of FeAlB tested in vacuum at 900 K, showing a mixture of transgranular cleavage fracture and intergranular cavitation.

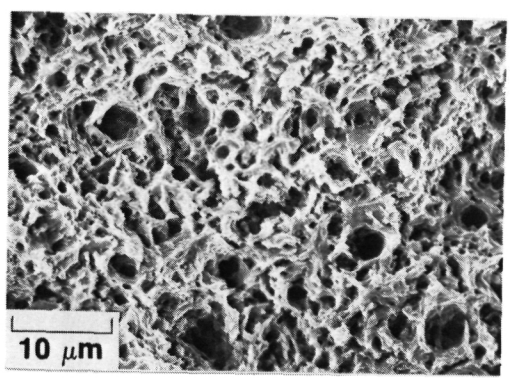

(a)

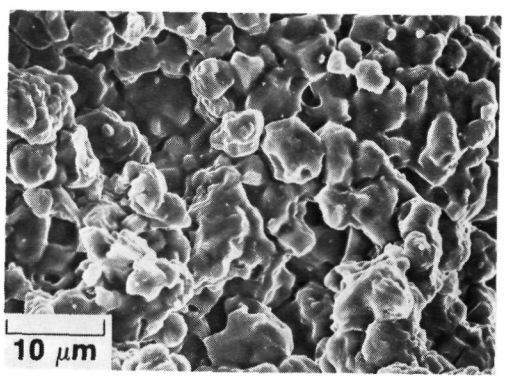

(b)

Figure 23. - SEM fractographs of FeAlZr tested in vacuum at (a) 900 K, showing complete cavitation, and (b) 1100 K, showing intergranular failure.

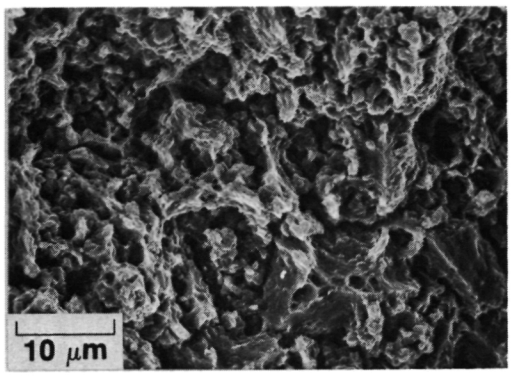

Figure 24. - SEM fractograph of FeAlZrB tested in vacuum at 900 K, again showing cavitation.

1. Report No.	2. Government Accession No.	3. Recipient's Catalog No.
NASA TM-87290		

4. Title and Subtitle	5. Report Date
Tensile Behavior of Fe-40Al Alloys With B and Zr Additions	6. Performing Organization Code: 506-63-01

7. Author(s)	8. Performing Organization Report No.
Darrell J. Gaydosh and Michael V. Nathal	E-2997
	10. Work Unit No.

9. Performing Organization Name and Address	11. Contract or Grant No.
National Aeronautics and Space Administration Lewis Research Center Cleveland, Ohio 44135 ND315153	13. Type of Report and Period Covered: Technical Memorandum
12. Sponsoring Agency Name and Address	14. Sponsoring Agency Code
National Aeronautics and Space Administration Washington, D.C. 20546	

15. Supplementary Notes

Prepared for the 1986 TMS-AIME Annual Meeting, New Orleans, Louisiana, March 2-6, 1986.

16. Abstract

Both Fe-40Al and Fe-40Al-0.1Zr with and without B were produced by the hot extrusion of powdered metal. Tensile properties were determined from room temperature to 1100 K in air. All of the materials possessed some ductility at room temperature, and addition of B caused an increase in ductility and a change in fracture mode from intergranular to transgranular cleavage. At high temperatures, failure was caused primarily by the formation of grain boundary cavities in all of the alloys. The effect of Zr addition was unclear because of the complexity of the various microstructures. Comparison of air and vacuum testing at high temperatures revealed that an apparent oxidation assisted mechanism reduced high temperature ductility in these alloys, especially at 900 K.

17. Key Words (Suggested by Author(s))	18. Distribution Statement
Iron aluminide; Ductility; B effect; Tensile behavior	Unclassified - unlimited STAR Category 26

19. Security Classif. (of this report)	20. Security Classif. (of this page)	21. No. of pages	22. Price*
Unclassified	Unclassified	21	

*For sale by the National Technical Information Service, Springfield, Virginia 22161